IEEE Access
Multidisciplinary | Rapid Review | Open Access Journal

Received 21 November 2023, accepted 26 December 2023, date of publication 2 January 2024,
date of current version 9 January 2024.

Digital Object Identifier 10.1109/ACCESS.2023.3349135

RESEARCH ARTICLE

Integrated Super Planar Inductor-Rectifier Design for EV Drive

SHAHID AZIZ KHAN[1], (Graduate Student Member, IEEE), YANGHE LIU[2], (Member, IEEE), MENGQI WANG[1], (Senior Member, IEEE), GUANLIANG LIU[1], (Student Member, IEEE), JAE SEUNG LEE[2], ABHILASH KAMINENI[3], (Member, IEEE), AND SHIVAM CHATURVEDI[1]

[1]Department of Electrical and Computer Engineering, University of Michigan-Dearborn, Dearborn, MI 48128, USA
[2]Toyota Research Institute of North America, Ann Arbor, MI 48105, USA
[3]Department of Electrical and Computer Engineering, Utah State University, Logan, UT 84322, USA

Corresponding author: Mengqi Wang (mengqiw@umich.edu)

ABSTRACT Power Density and cost are the key design criteria for the modern power electronics unit in Electric Vehicles (EVs). EVs widely adopt inductive wireless charging technology, which contains the receiving coil and the AC-DC converter on the vehicle side. However, the vertical space on the chassis for charging electronics is very limited. Moreover, with a non-compact package comes a high damaging probability due to unpredictable road conditions, higher costs, and vehicle integration issues. This research presents the concept of distributed planar magnetics with the integrated rectifier hardware design for the vehicle side charging electronics by combining the concept of planar-distributed magnetics with the design space optimization research. A planar-distributed inductor module consisting of 16 EI cores with PCB-embedded windings was designed, modeled (using a novel high-fidelity model), and fabricated using the design space optimization technique, which resulted in a 66% increase in the power density. This research treated and solved the power density problem as an optimization problem considering every constraint involved and presented a thorough investigation from the design space utilization, power loss, loss and frequency relation along with the magnetostatic and electrostatic analysis perspective. It also provides a comparative study of various materials for the inductor fabrication keeping in view the automotive application environment. Moreover, a hybrid approach (metalcore and FR4) PCB was used instead of a regular FR4 PCB after an in-depth study and performance comparison.

INDEX TERMS Electric vehicles, wireless charging, power density, power converters, planar inductor, distributed magnetics.

I. INTRODUCTION

Electrified transportation is considered a major breakthrough in tackling global climate change and Carbon emissions. Electric Vehicles are the backbone of the transition towards clean energy and meet the zero-emission targets [1]. Recently EVs have been developed significantly in terms of performance and drive range. However, EVs' current global charging infrastructure cannot meet the demand. The development of plug-in hybrid and battery electric vehicles demands charging infrastructure. The goal is to replace conductive charging with wireless charging, and the long-term objective is to power the moving vehicles on the road. Once accomplished, it will result in a light battery pack but an extended driving range. The charging technology can be divided into wired or contact charging and wireless or non-contact charging. The first is a traditional and mature method, while the wireless technique is a new technology. Usually, radio transmission technology is utilized for wireless power transfer (WPT) [2]. Radio transmission technology can transmit energy in three ways: inductive transfer, resonant and microwave transmission. Inductive charging is mostly

The associate editor coordinating the review of this manuscript and approving it for publication was Zhehan Yi.

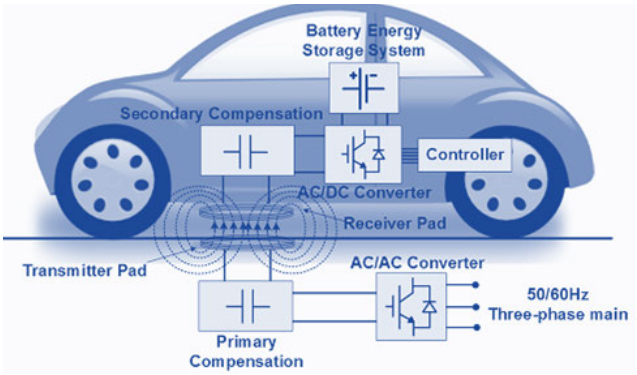

FIGURE 1. Inductive wireless power transfer (wpt) methodology.

used for vehicle charging due to its benefits. It's a loosely coupled structure similar to a separable transformer, which transfers the energy from the grid to the onboard chargers in close proximity, shown in Figure 1. There is no direct contact between the vehicle and the grid. The air gap isolates the grid side WPT transmitting pad and the vehicle side receiving coil.

The WPT transmitting pad is isolated and separated through the air gap on the grid side. Due to the absence of any contact and connectors, inductive wireless charging is very safe, convenient, and user-friendly. The resonant power transfer technique can be applied using near-field magnetic resonance coupling. Microwave a radiant energy transfer, with a lower efficiency with far-field and possess the risk of harming human health; therefore, it's not a strong candidate for commercial EV wireless charging technology. All the major automotive players, such as Tesla, Toyota, Ford, ZTE Corporation, etc., have already demonstrated their WPT technology and are racing to develop and commission the wireless charging infrastructure for their EVs [3]. The global EV wireless charging market is predicted to reach USD 221 million by 2028 [4].

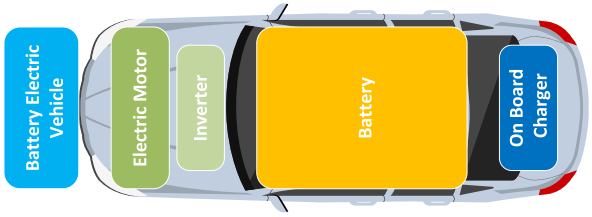

FIGURE 2. Battery electric vehicle architecture.

The battery electric vehicle is architecture differs from the traditional combustion engine vehicles. Figure 2 shows the battery electric vehicle architecture where it can be seen that in the EV majority of the space is taken by the battery pack, and the remaining space needs to be distributed among motors, inverters, and onboard chargers. Thus EVs incur distinct packaging constraints to adjust electrified powertrain. Finding the optimal balancing point between the large battery size and the small vehicle size (to attain a longer driving range) is a design challenge. The design freedom aided by the lack of requirements for the driveline tunnel and combustion compartment, which was used to expand the cargo and passenger space, further shrinks the area available to the electronic traction drive system (ETDS) components in the chassis near the steering and suspension and away from the crash zones. An increased power density is the only solution to these constraints and to realize a skateboard chassis design with a widespread electrification platform. Figure 3 presents the distribution of ETDS components on the chassis [5], [6]. The major automotive manufacturers, such as Ford, Lucid, Tesla, General Motors, Volkswagen, etc., have shown significant interest in using electric drive vehicles for mobility as a service application. The 2025 technical targets published by the US Department of Energy (DOE) aim to reach a power density of 33KW/L for a 100 KW traction drive system, which is an increase by a factor of 5.5 and an 88 percent volume reduction compared to the state of the art technology [7], [8].

To the best of the author's knowledge, this is the first paper to combine the concept of planar and distributed magnetics considering the design space optimization constraints, therefore contributing to the increasing power density and magnetics design space optimization research.

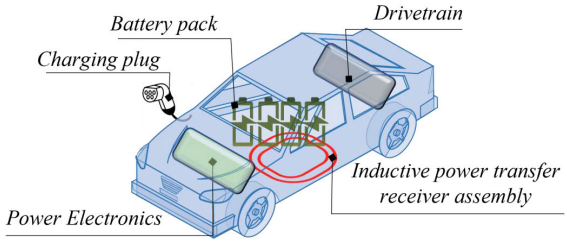

FIGURE 3. Battery electric vehicle architecture.

While it is commonly known that higher switching frequencies lessen the need for energy storage on magnetic components [9], [10], the ideal magnetic component's size is a more complex issue [11]. A number of factors, including winding losses, permeability of magnetic materials, core losses, and temperature and heat transfer restrictions, must be taken into account in order to size magnetic components effectively [12]. Furthermore, the automation and repeatability of power electronic systems are hindered by the labor-intensive production complexity linked to conventional Litz wire and copper foil-based windings [13]. Features of low-profile planar magnetic components, like higher power density, superior thermal performance, unparalleled repeatability and modularity, ease of manufacturing, and predictable parasitics, have become increasingly popular with the rapid advancement of printed circuit board (PCB) technology [14].An inductor in series with the isolation transformer is necessary for many common high-power isolated DC-DC converter topologies. Integrating this series inductance as a programmable leakage of the

isolation transformer further reduces the cost and boosts the power density of such converters [15]. Since the leakage flux is contained in the air, attempts to create additional leakage inductance by increasing the spacing between the primary and secondary windings in the core window are not very successful in producing a well-defined leakage inductance [16]. They also result in a reduction of core utilization. Alternative strategies for demonstrating the integration of a programmable inductor with the isolation transformer employing unique core structures can be found in the literature currently in publication [17], [18]. A definite trade-off has been shown between component efficiency, power density, and manufacturing complexity in all of the integration strategies now in use. Perfect interleaving between a transformer's primary and secondary must be broken in order to enable the creation of programmable leakage inductance, which subsequently leads to higher AC winding losses [19]. A definite trade-off has been shown between component efficiency, power density, and manufacturing complexity in all of the integration strategies now in use. Perfect interleaving between a transformer's primary and secondary must be broken in order to enable the creation of programmable leakage inductance, which subsequently leads to higher AC winding losses. For high-frequency planar magnetic designs with PCB-embedded windings, this technique is highly appealing because of the flexibility of routing in PCB-based winding implementation. There are two ways to design and regulate the leakage inductance in this technique, which leads to very different tradeoffs when looking at winding and core loss. For low power levels, especially in RF applications, the concept of integrated and distributed magnetics is common, but here the application is different and involves 2.5KV AC input at 100KHz on the primary side, which converts to 600V AC at 100 KHz on the secondary side. For the rectifier, the output should be around 400V and 18A to power the required load. This work increases the overall power density of WPT electronics on the vehicle side by reducing the height of the filtering network inductor, which is a bottleneck for enhancing the power density.

The key contributions of the paper are defined as follows.

1) It solves the problem of the large size of the filtering inductor associated with the rectifier stage by adopting a distributed and planar integrated magnetics approach, which is not common for such high power levels.

2) There is an upper limit up to which the size of the magnetics can be reduced by increasing the frequency due to the thermal management challenges. This research proposed a design space optimization framework for high-frequency distributed magnetics to find the optimal placement considering thermal and magnetic aspects.

3) Instead of using the traditional magnetic equivalent circuit (MEC), a high-fidelity magnetic equivalent circuit was used to model and manufacture the inductor. This approach reduces the uncertainties associated with the traditional model by accurately modeling the airgap fringing fluxes.

The paper is organized as follows: The introduction section provides a deep overview of the problem statement along with the literature review and highlights the contributions of this paper. Section II focuses on the understanding of the vehicle side power electronics which is necessary to comprehend the problem solved through this research. Section III explains the methodology and the proposed high-fidelity modeling technique for the planar inductor design. Based on the mathematics explored, Section IV presents the magnetostatic and electrostatic analysis to prove the effectiveness and correctness of the proposed modeling technique along with the justification of the material chosen for inductor fabrication through a comparative study. Section V is focused on the experimental results along with the new key findings of design space optimization, which is crucial for the distributed magnetics approach. It also presents the various parameters and their relationship and how they can affect the performance and functionality of the integrated planar inductor module. The details of the test setup and circuit schematics are provided followed by the experimental results.

II. VEHICLE SIDE WPT ELECTRONICS

The electronic structure for the WPT technology can be divided into two sides: The grid side and the vehicle side. On the grid side, the first stage is to convert the AC power into DC power using an AC-DC converter integrated with a power factor correction (PFC) circuit. The next step involves the conversion from DC power to a high-frequency AC to power up the coil on the transmission side through a compensation network. An isolation transformer is usually used between the converter and the coil for safety. An alternating magnetic field is generated in the transmitting coil due to the high-frequency current, which induces a voltage on the receiving coil. The compensation network on the secondary side improves efficiency. The last stage, also the one which this paper is focused on, is the rectification stage to charge the battery [20], [21]. This configuration is presented in figure 4.

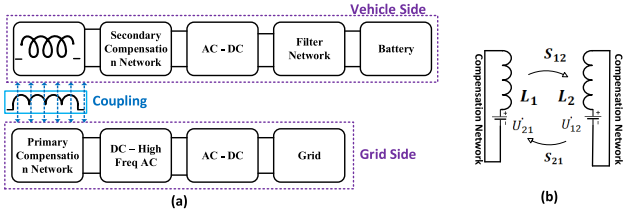

FIGURE 4. (a) WPT system block diagram (b) WPT power transfer.

Mathematically, the power transfer through the coil can be represented as [22] and [23]

$$\begin{aligned}\dot{S}_{12} &= -\dot{U}_{12}\dot{I}^*_2 = -j\omega M\dot{I}_1\dot{I}^*_2 \\ &= \omega M I_1 I_2 \sin\varphi_{12} - \omega M I_1 I_2 \cos\varphi_{12} \qquad (1)\\ \dot{S}_{21} &= -\dot{U}_{21}\dot{I}^*_1 = -j\omega M\dot{I}_2\dot{I}^*_1 \\ &= \omega M I_1 I_2 \sin\varphi_{12} - j\omega M I_1 I_2 \cos\varphi_{12} \qquad (2)\end{aligned}$$

$I1$ and $I2$ are the RMS value and the $\varphi 12$ is the phase difference. Then the power transfer from the primary to the secondary side is modelled as

$$P_{12} = \omega M I_1 I_2 \sin \varphi_{12} \tag{3}$$

To represent the total complex power transfer from one side of the coil to another we assume $\varphi_1 2 = pi/2$, and the active power can be transferred in both directions then the total complex power is given by

$$\begin{aligned} \dot{S}_{12} &= \dot{S}_1 + \dot{S}2 \\ &= j(\omega L_1 \dot{I}_1 + \omega M \dot{I}_2)\dot{I}^*{}_1 + j(\omega L_2 \dot{I}_2 + \omega M \dot{I}_1)\dot{I}^*{}_2 \\ &= j\omega(L_1 {I_1}^2 + L_2 {I_2}^2 + 2 M I_1 I_2 \cos \varphi_{12}) \end{aligned} \tag{4}$$

Similarly, the reactive power can be expressed as,

$$Q = \omega(L_1 {I_1}^2 + L_2 {I_2}^2 + 2 M I_1 I_2 \cos \varphi_{12}) \tag{5}$$

After the primary side generates the high-frequency current into the sending coil through a converter, a rectification stage is implemented on the secondary side [24], [25], [26], [27]. As the focus here is the secondary side converter i.e. rectifier. The role of the rectifier design becomes very important when a secondary side control [28], [29] or a dual side control [30] architecture is adopted. After the rectifier, a boost converter is inserted for the control in the case of a parallel compensation also depicted in figure 5. However, in the series compensation scenario, a buck converter can be utilized. Moreover, the filtering and compensation network is also required. the bottom line is that no matter what control strategy we adopt the presence of the bulky inductor cannot be avoided, which is a design challenge that this research resolved.

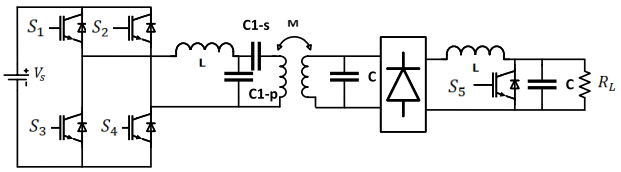

FIGURE 5. Circuit schematics of WPT configuration.

This research focuses on a super planar inductor design integrated with the rectification stage. The research was carried out with an automotive industrial partner where the actual space available on the chassis of the electric vehicle was measured and then the targets were set. The vertical space available on the chassis is very limited so the design needed to be spread horizontally. For this purpose, a novel approach was adopted. Instead of using and combining the market components, an EI-inductor was designed from scratch and fabricated and placed on the board in a series connection. Moreover, less height and more width can result in a weak structure and poor thermal performance (limitation of heat sink), which was resolved by doing an in-depth comparison of different PCB material's performance and comparison.

TABLE 1. Various options for EI core design and manufacturing.

Options	Plan Details	Core Winding	Cost	Height	Performance
Option 1	Self Design Best material	Customized Soft Core + PCB Windings	Highest	$1\sim 2cm$	1st
Option 2	Self Design Traditional Material	Available Ferrite Core + PCB Windings	3rd	$1\sim 2cm$	2nd
Option 3	Design by Manufacturer	Ferrite Core +Copper Windings	2nd	$3\sim 4cm$	3rd
Option 4	Available on Market	Common Core +Copper Windings	Cheapest	6 cm	4th

Finally, the metal core PCB was found to be the best one in terms of structural reliability and thermal performance. Table 2 compares different EI-inductor approaches that can be opted for. However, remember the objective is to have an inductor with the least height to attain maximum power density and reliability.

III. MULTI-PLANAR INDUCTORS DESIGN

Using planar magnetic in power electronics applications ensures high power density, improved thermal performance, ease of manufacturability at large scale, and predictable parasitic parameters. Usually, the planar magnetic core uses a ferrite core with lamination layers. The traditional magnetic components with copper and litz wire windings have many limitations, such as bulky size, power loss, and complex fabrication methods [31]. The planar magnetics design with PCB windings is a good candidate to overcome these inherent issues. The planar magnetics also helps to achieve the best thermal performance as they enlarge the heat dissipation area. Due to the proximity of the primary and secondary windings, the overall power loss profile is improved due to the mitigation of loss phenomena such as eddy current, etc. Automatic production and high efficiency can be achieved simultaneously through planar magnetics; however, the issue of large volume and number still exist. To overcome this, an integrated approach is followed in this research where a planar EI-core inductor was designed and then placed in series with identical inductors to form an inductor board or module to achieve the required inductance and thermal performance and then integrated with the converter compactly. This distributed magnetics approach can effectively shrink many magnetic components, improving power density. Figure 6 shows the planar inductor design with the PCB-embedded windings.

A. EI-CORE DESIGN MODEL

This research demonstrates an improved version of the distributed EI cores structure that contains a new air gap at

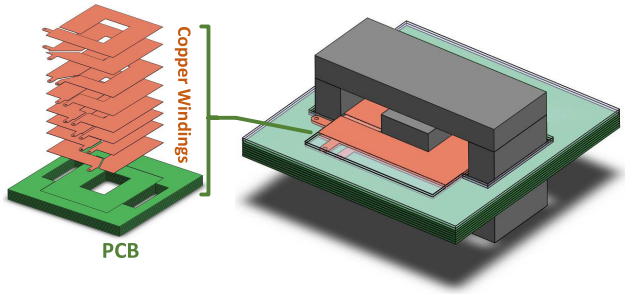

FIGURE 6. Planar inductor with embedded PCB windings.

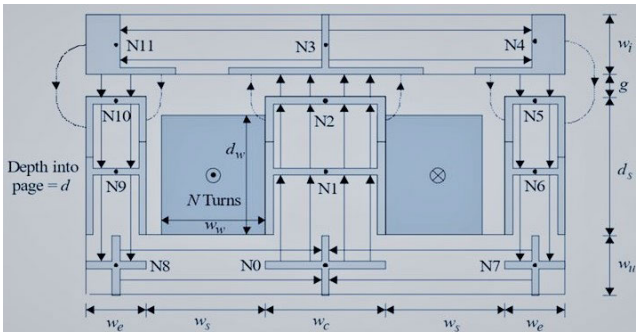

FIGURE 7. EI-core structure labeled for modeling.

the center leg of the E-core. It is to be noted that the value of the inductance will rely on the area of this air gap, which is helpful for multiple applications, as the desired inductance can be achieved by modifying the length of the air gap and the cross-sectional area. This research also optimises the planar inductors' distribution in the available design space. Figure 7 shows the EI core inductor structure. d_s is the slot depth, w_s is the slot width, d_w is the winding depth, g is the airgap, N refers to the number of turns, w_t is the wire type, w_i is the I-core width, w_e is the E-core width, w_u is the E-core center width, w_u is the E-core underside width and d is the depth to which the inductor core extends into the page. Instead of using the normal and traditional modeling approach, here, a high-fidelity magnetic equivalent circuit (HEMEC) model is used. Compared to the traditional magnetic equivalent circuit (MEC) model approach, this model reduces the inaccuracies associated with the traditional method [32]. The area of the column is the sum of the areas of two sides legs for an EI-type magnetic core, presented mathematically in Eq 6.

$$w_c = w_e + w_e = 2w_e \tag{6}$$

The HFMEC of the EI core is shown in Figure 8. The inductor geometry shown symbolizes the flow of current into the page and the circular dot represents the current flow in and out of the page through the conductors with width w_w and height d_w. When inserted into a PCB the winding is wrapped around the centre post resulting in an magnetive motive

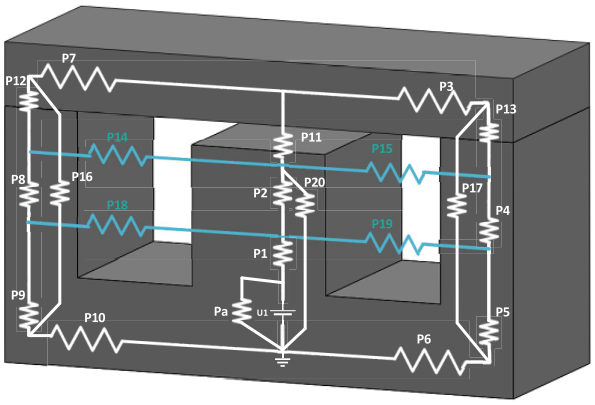

FIGURE 8. High fidelity magnetic equivalent circuit model.

force (MMF) source described by the Eq.7.

$$F = Ni \tag{7}$$

N is the number of turns and i is the flowing current. The permeance of the *kth* branch of the HEMEC can be defined using the core material, core geometry, and winding current as,

$$P_k = \frac{(A_k)}{(L_k)}\mu(.) \tag{8}$$

A_k is the magnetic flux cross-sectional area, L_k is the path length, and μ is the absolute permeability. The HEMEC model consist of straight core permeances($P_1 - P_{10}$), airgap permeances ($P_{11} - P_{13}$), and leakage permeances ($P_{14} - P_{20}$). The important difference between the traditional MEC and a HEMEC is the calculation of the air gap and leakage permeances. Table 2 shows the categorization of the permeances for better understanding.

TABLE 2. Permeances categorization for HEMEC.

Permeance Categorization	Straight Permeances	AirGap Permeances	Leakage Permeances
Permeance Element	$P_1 - P_{10}$	$P_{11} - P_{13}$,	$P_{14} - P_{20}$

B. AIR GAP PERMEANCES CALCULATION

The air-gap permeances were calculated using a standard method presented in [33]. Moreover, when the magnetic flux passes through the air gap between E and I cores, it causes a fringing effect [34]. The permeance equations can be stated as

$$P_{12} = P_{13} = P_{of} + P_{if} + P_{bf} + P_{ff} + P_{gf} \tag{9}$$

$$P_{11} = 2P_{if} + P_{bf} + P_{ff} + P_{gf} \tag{10}$$

and,

$$P_{if} = \frac{\mu_o d}{\pi} \ln|1 + \frac{\pi\omega_i}{g}| \tag{11}$$

$$P_{of} = \frac{2\mu_o d}{\pi} \ln|1 + \frac{\pi\omega_i}{4g}| \tag{12}$$

$$P_{bf} = P_{ff} = \frac{\mu_o \omega_e}{\pi} \ln|1 + \frac{\pi \omega_i}{g}| \quad (13)$$

$$P_{gf} = \frac{\mu_o \omega_e d}{g} \quad (14)$$

The leakage permeance elements $P_{14} - P_{20}$ correspond to the flux traveling outside the core's magnetic path. P_{14} *and* P_{15} corresponds to the horizontal flux, P_{16} *and* P_{17} corresponds to the verticle flux and the remaining components $P_{18} - P_{20}$ corresponds to vertical and horizontal fluxes. The leakage flux calculations can start from the field intensities calculation for the EI core utilizing Ampere's law. The horizontal leakage permeance corresponding to the elements $P_{18} - P_{19}$ in HFMEC model can be writtenas,

$$P_{18} = P_{19} = P_{xs}|0 <= y <= d_w + 2P_{xf}|0 <= y <= d_w = \frac{\mu_o d_\omega d}{3\omega_s} + \frac{2\mu_o d_\omega}{3\pi} \ln|1 + \frac{\pi w_c}{2w_s}| \quad (15)$$

$$P_{14} = P_{15} = P_{xs}|d_w <= y <= d_s w + 2P_{xf}|d_w <= y <= d_s = \frac{\mu_o d}{\omega_s}(d_s - d_w) + \frac{2\mu_o (d_s - d_w)}{\pi} \ln|1 + \frac{\pi wc}{2w_s}| \quad (16)$$

The vertical leakage permeances P_{16} and P_{17} are as follows

$$P_{16} = P_{17} = \frac{\mu_o d(\omega_s - \omega_w)}{d_s + g} \quad (17)$$

$$R = \frac{\omega_t + \omega_b}{\mu_o \omega_t \omega_b \omega_c}[\omega_w + \sqrt{\frac{(2d + \omega_t + \omega_b)\omega_t \omega_b}{\omega_t + \omega_b}}] \quad (18)$$

$$P_{20} = 2(P + R^- 1) \quad (19)$$

IV. INDUCTOR SIMULATION AND MANUFACTURING

Considering the application requirements, available space at the chassis of the vehicle, and the mathematics explained in the previous section, the inductor was simulated in ANSYS/Maxwell workbench. Apart from the super planar design and geometry, the contribution points of this inductor design include

1) Using individual design for each inductor to adjust the heat loss to realize the balance heat distribution, as the different inductor's locations can cause an imbalance in heat distribution.
2) Avoiding the interface between two different inductors, as two closed inductors can cause mutual inductance which will result in the reduction of the inductance value.
3) Careful performance evaluation of the Nano-materials. Table 3 shows the comparison of the nanocrystalline material which was evaluated.

Computing the power losses before finalizing the inductor design parameters is important. Here the focus is on calculating the copper loss and core loss. Winding resistance helps in the calculation of copper power loss.

$$R_w = \frac{\rho l_w R}{A} \quad (20)$$

TABLE 3. Nanocrystalline material comparison.

Mate	Plan	Core	Cost	Height	Pere	Perf	Pence
Saturation Flux Density Bs (T)	2.03	0.5	1.55	0.74	0.58	1.56	1.25
Coercivity Hc (A/m)	40	8	12	2.4	0.4	2.4	1.2
Initial Permeability (μ_i)	1500	3000	6000	40000	100000	5000	80000
Max Permeability (μ_m)	20000	6000	60000	200000	1000000	50000	400000
Electrical Resistivity ($\mu\Omega_{cm}$)	50	5x10^7	30	60	140	130	115
Curie Temperature (C)	750	220	550	450	250	399	570

ρ is the resistivity of the material for conductor, $l_w R$ is wire length and A is the cross-sectional area.As for this rectifier application, the rated current is $18A$, so the power loss comes out to be $2.5W$. For the core loss calculation according to this application and the working conditions i.e. at $13KHz$ and $77g$ for each inductor, Equation 21 can be used to calculate the core loss which turns out to be $4.5W$.

$$P_{core} = K_{1f}^x B^y V_e \quad (21)$$

whereas, $K1$ =core material constant, f = frequency(kHz), B = $PeakFluxdensity$, x = frequency exponent, y = flux density exponent, and V_e = Effective core volume. The overall dimensions of our designed inductor are $40 \times 20 \times 15(mm)$.

The inductor was simulated with different airgaps to check the airgap sensitivity. Due to the higher magnetic conductivity, it was established that the design air gap length should be strictly limited to under 0.05mm. Figure 9 shows the inductor behaviour for $0.05mm$ airgap. In figure 9(a) the power loss of the whole planar inductor geometry is simulated. The flux linkage, associated induced voltage and the resultant core loss are presented in figure 9 (b).

Another important aspect of the magnetics design is the magnetic field strength and energy estimation depicted in Figure 10 (a) and Figure 10 (b), respectively on a logarithmic scale for better understanding. Planar winding design plays an important role in the overall performance of the designed planar magnetic component. The copper thickness, insulation thickness, structural geometry, etc., are all important factors involved in the winding design. The current density analysis was performed to determine the designed winding's performance for this research. Figure 11 (a) shows the magnetic field distribution, and Figure 11 (b) shows the current density of the PCB windings. The current density distribution is not as uniform as expected due to the proximity and skin effects. The total loss that

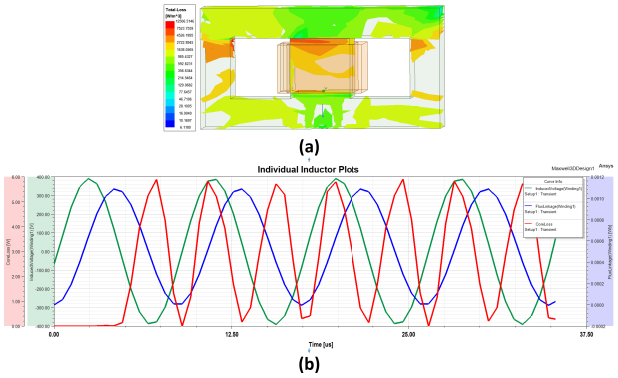

FIGURE 9. (a) Power loss analysis (b) Core loss, induced voltage and flux linkage waveform.

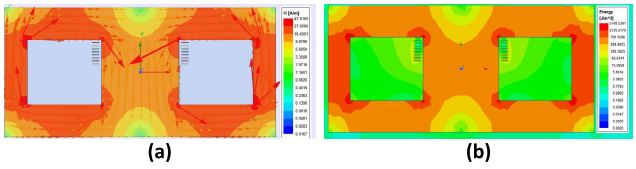

FIGURE 10. (a) Magnetic field strength (b) Energy.

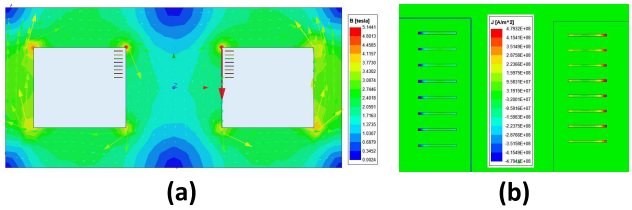

FIGURE 11. (a) Magnetic field distribution (b) Current density distribution of PCB windings cross section.

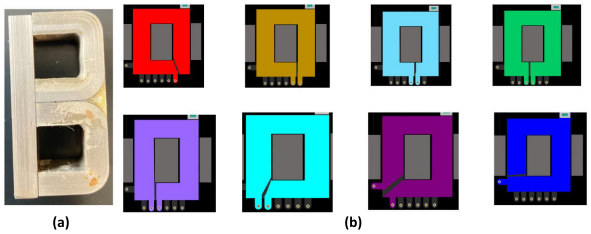

FIGURE 12. (a) Manufactured inductor (b) Designed PCB windings.

occurs across the inductor is the combination of the core loss, windings loss, and the loss due to these effects.

Figure 12 shows the manufactured inductor and the designed PCB Winding. An eight-layer FR4 PCB was used for the windings design of the proposed inductor, as a result, the fabricated PCB that contains the inductor windings is very thin, which offers improved window area leading to better thermal and magnetic performance.

V. EXPERIMENTAL RESULTS

The simulation results of the modeled and manufactured inductors are shown in the previous section. Instead of

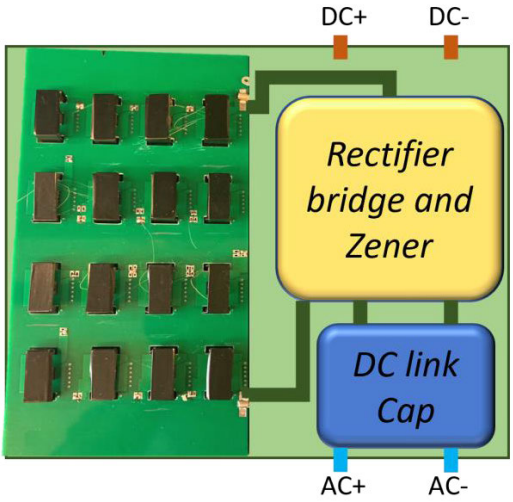

FIGURE 13. Metal core and FR4 board combination to form a rectifier stage integrated with distributed planar inductor module.

using a single inductor for the experimental verification, based on the required power level of the application here, an inductor module board was developed containing sixteen planar distributed inductors shown in Figure 13. It can be seen that the inductor modules board, which acts as a high power density single inductor, is attached to the rectifier circuit; the circuit is blurred or animated due to the intellectual property of the industrial research partner involved in this research.

For a better understanding of the considered rectification stage, Figure 14 presents the simplest representation of the schematics. This work is focused on the highlighted load side inductance. The schematic design represents the stage in the wireless power transfer system on which this research is focused i.e. the rectification and filtering stage on the vehicle side. It means the input AC signal comes from the secondary compensation network integrated with the wireless transfer coil. High-frequency AC power is wirelessly sent to the secondary coil via the mutual inductance between the primary and secondary coils. To enhance the transfer efficiency, the secondary compensation network and secondary coil must be set to have the same resonance frequency. After

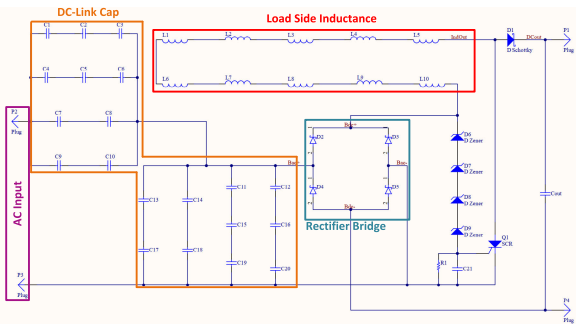

FIGURE 14. Schematics design of the rectification and filtering stage.

passing through the rectifier stage and the filter network, the high-frequency AC power is converted to DC power. At last, the battery pack can be charged using DC power.

Distributed magnetics are complex to handle as many design variables are involved, such as the gap between individual magnetic components, mutual inductance, arrangement geometry, and thermal aspects. The goal is to optimize the available design space for better thermal and electromagnetic performance. Different techniques can be adopted for allocating and optimizing the design space, ranging from simple mathematical distribution to complex algorithms. This research area of design space optimization for magnetics is still evolving. Here an algorithmic approach was adopted, and multiple valid solutions can be achieved based on the targets. It's upto the design engineer to select the solution that results in better overall performance, including reliability, power density, easy integration, and cost.

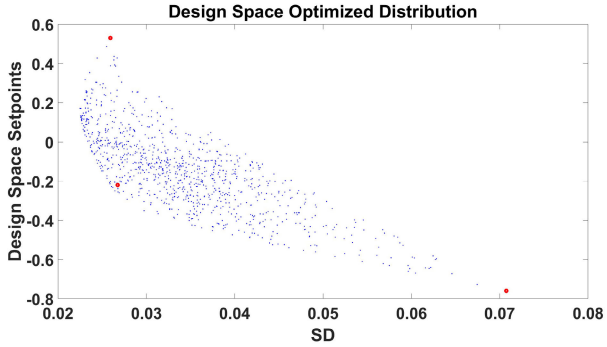

FIGURE 15. Design space optimized distribution.

Figure 15 presents the obtained design optimization scenario where a relation between the design space setpoints and standard deviation (SD) was established that resulted in various solutions. The design space optimization aims to identify the optimal solution among the possible solutions. Various constraints, such as the minimum and maximum distance between two individual inductors, the total area of the inductor module board, overall temperature, mutual inductance and self-inductance etc., are the constraints that control the possible solutions. Choosing the best solution manually is difficult and prone to errors; however, establishing a relationship that contains the input from all the parameters involved makes the decision-making fast, accurate and easy. This article focuses more on magnetic modeling and design, so discussing the adopted algorithm is beyond the scope and focus. A point corresponding to the positive value on the y-axis and with the lowest standard deviation can be considered a good solution.

Mutual inductance among such distributed magnetic components is crucial to consider, and it can significantly affect the performance. In an available design space, multiple orientations can result in various values for mutual inductance. Thus, quantifying the mutual inductance is a complex but necessary step for efficient design decision-making.

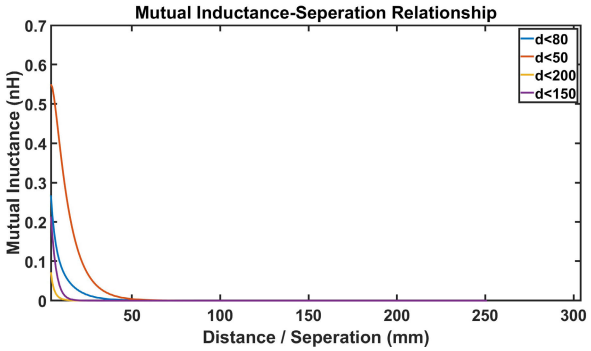

FIGURE 16. Mutual inductance and mutual separation distance.

However, as this kind of distributed magnetics approach is not common and is still an evolving research field, a relation between the separation between the planar inductors and the mutual inductance was derived for the design of the planar distributed inductor module, as shown in Figure 16 ensure an optimized distribution in the available design space. It can be observed that the mutual inductance varies with the change in the distance. However, the variation is not linear or too simple to be extrapolated. Hence, a relationship between the separation distance and mutual inductance was essential and very helpful.

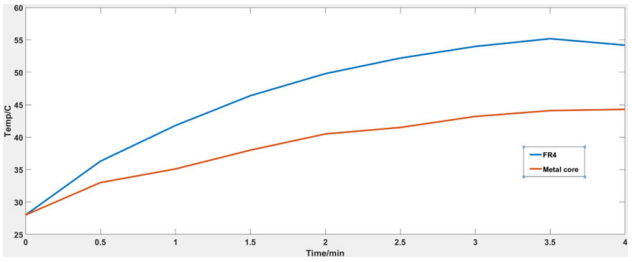

FIGURE 17. Metal Core vs FR4 board thermal performance comparison.

According to the application, an inductor module board was developed for experimental validation and verification to attain the inductance value. The operating environment in the vehicle chassis is harsh and leads to high temperatures. Moreover, the rectifier board generates its own heat due to the associated power dissipation. An in-depth comparison of different PCB material's performance and comparison was carried out. Finally, the metal core PCB was the best in terms of structural reliability, cost and thermal performance. After different test combinations, it was established that a dual approach that uses the metal core PCB for the rectifier board and FR4 PCB for the inductor board module is the optimal choice considering weight, cost, reliability, and thermal performance. The thermal performance curves obtained after the test to compare the performance of the metal core and FR4 PCB are presented in Figure 17. It can be observed that the metal core PCB (red curve) provides better thermal performance compared to the conventional FR4 PCB (blue curve), which supports the proposed design methodology

of using a hybrid combination which yields better overall thermal performance.

To analyze the working of the designed planar and distributed inductor module, a frequency sweep analysis was performed with respect to the solid loss. The current can vary in different conditions for this wireless power transfer-based inductive charging application as the current flowing through the inductor can vary based on the region and type of charging. Analysis was done to test the magnetic performance under different current conditions, resulting in the fact that the solid loss increases with the increase in the frequency. The current, as well as the frequency, was varied for a wide range to observe the loss characteristics. Usually, the magnetics are tested and analyzed for a specific frequency and current, making the analysis less beneficial for researchers. Here, a very broad and detailed analysis was done with the aim of extending this result to other magnetic geometries and applications. Using this analysis, the design engineer can conclude the limitations of the designed electronics and take the required thermal dissipation measures.

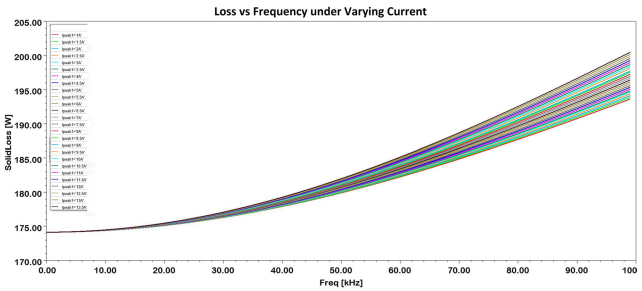

FIGURE 18. Dynamic performance under varying current and frequency.

Figure 18 presents the analysis performed under changing current scenarios. The experimental setup was tested on different frequencies, and the corresponding core loss was measured to note the behavior of the magnetic core. The resultant relationship between the core and frequency shown in Figure 19 is very similar to the results obtained through the FEA analysis, which shows the accuracy of the design. Core loss is an important factor to measure and verify when the design involves magnetics, as it leads to the critical decisions of designing the thermal dissipation strategy and estimating the system efficiency.

The experimental test bench is presented in Figure 20 where it can be seen that the setup consists of the AC input source, the rectifier stage integrated inductor module board connected to the load. A current probe is utilized for the output current measurement. The temperature is measured continuously through a thermal camera device to ensure and analyze the required thermal performance. Figure 21 shows the waveforms from the experimental setup. The output voltage is 91.2V with 9.8A of current. The input voltage is set at 102.8V; the difference between the input and output voltage presents the associated power loss at this rectification stage. The experimental setup consists of an AC input source

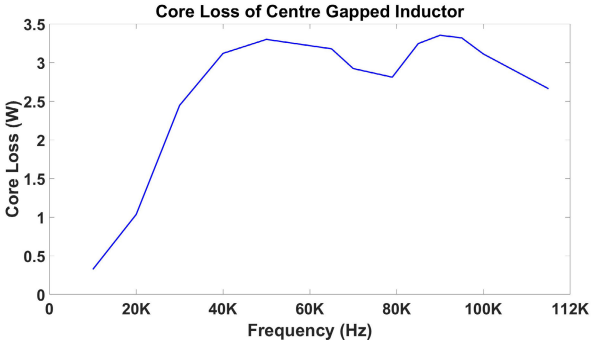

FIGURE 19. Core loss and frequency relationship.

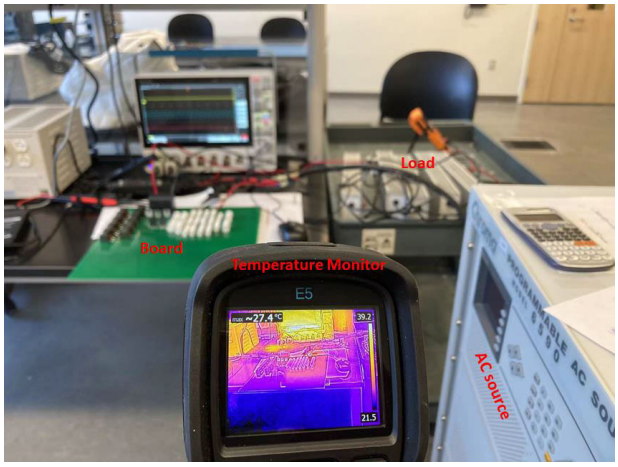

FIGURE 20. Test Bench for testing the integrated and distributed planar inductor-rectifier.

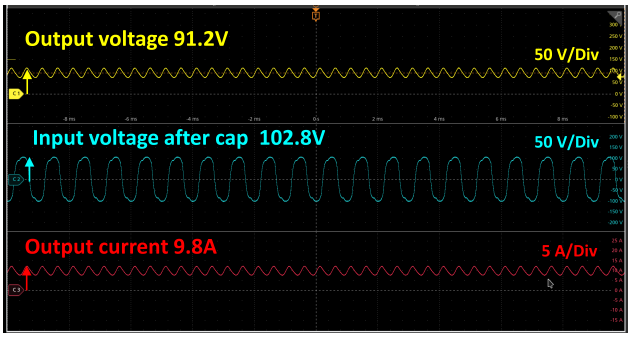

FIGURE 21. Rectifier Stage with integrated inductor module experimental results.

emulating the stage after the secondary side compensation network in the WPT vehicle side electronics. The inductor module board integrated with the rectifier and connected to the resistive load is tested for functionality. The rectifier stage result shows that integrating the inductor module and rectifier stage board works well, achieving the required rectification.

Another major goal of this research was to increase the power density, so the designed planar inductor's module

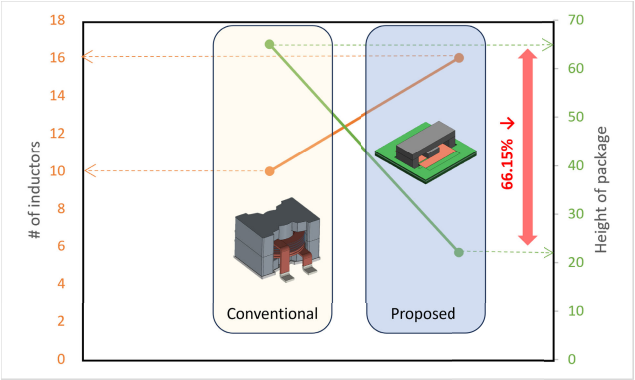

FIGURE 22. Compariosn of designed inductor package height vs conventional one.

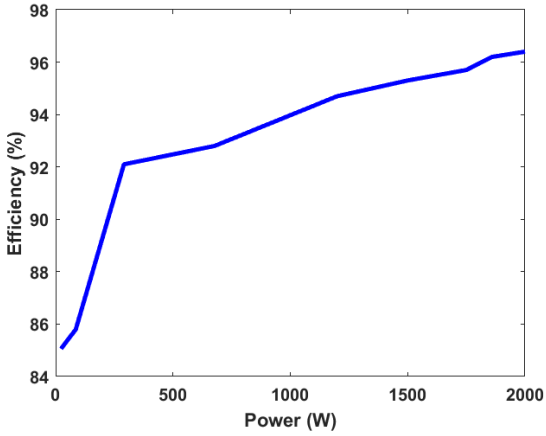

FIGURE 23. Experimentally measured efficiency of the proposed and designed system at various power levels.

height (22mm) was compared with a conventional package(65mm), capable of operating in the same operating conditions and offering similar inductance value and a decrease of 66% in package height was observed as depicted in Figure 22, which solved the problem of the limited verticle space in the chassis of the EV. The distribution of low-profile passive components with better heat dissipation from metal core PCB mainly contributes to the power density increase. The comparison is based on the whole inductor module board integrated with the rectifier stage and contains sixteen individual inductors arranged based on the presented design space optimization approach and connected electrically forming a distributed planar magnetics concept.

The experimentally measured efficiency plot of the system is given below in Figure 23. As this work is focused on improving the power density and no new circuit topology is proposed, so compared to the traditional efficiencies presented in the literature for this stage in the WPT system, the measured efficiency here is similar [35]. From the graph, it is evident that the efficiency increases when the testing power level is increased.

VI. CONCLUSION

In Conclusion, this research solved the problem of limited vertical space on the electric vehicle chassis for WPT power electronics by modeling and designing super planar-distributed magnetics with integrated PCB windings considering the design space optimization constraints. A novel and more accurate high-fidelity model was derived instead of using the available and traditional magnetic equivalent circuit (MEC) models that helped to model the magnetic component behavior accurately. Overall, this research treated and solved the power density problem as an optimization problem considering every constraint involved, resulting in a significant 66% increase in power density. Moreover, the combination of a metal core and FR4 PCB was used based on the test data for optimal thermal performance. This research paves the way for developing a high-power density WPT power electronics unit. It is also a step forward in distributed magnetics and automated magnetics design, an evolving research area for which the concept of explained design space optimization is essential.

REFERENCES

[1] B. Jones, R. J. R. Elliott, and V. Nguyen-Tien, "The EV revolution: The road ahead for critical raw materials demand," *Appl. Energy*, vol. 280, Dec. 2020, Art. no. 115072.
[2] L. Shuguang and J. Jia, "Review of EV's wireless charging technology," in *Proc. IEEE 2nd Int. Conf. Electron. Commun. Eng. (ICECE)*, Dec. 2019, pp. 128–132.
[3] G. Palani, U. Sengamalai, P. Vishnuram, and B. Nastasi, "Challenges and barriers of wireless charging technologies for electric vehicles," *Energies*, vol. 16, no. 5, p. 2138, Feb. 2023, doi: 10.3390/en16052138.
[4] Fortune Business Insights. (2022). *Electric Vehicle Wireless Charging Market Size [2021–2028] Worth USD 221.0 Million | Exhibit a CAGR 42.4. Retrieved From*. [Online]. Available: https://www.globenewswire.com/en/news-release/2022/03/22/2407707/0/en/electric-vehicle-wireless-charging-market-size-2021-2028-worth-usd-221-0-million-exhibit-a-cagr-42-4.html
[5] X. Chen, C. Gu, J. Yin, F. Tang, and X. Wang, "An overview of distributed drive electric vehicle chassis integration," in *Proc. IEEE Conf. Expo Transp. Electrific.*, Aug. 2014, pp. 1–5.
[6] C. Liu, C. Jiang, and C. Qiu, "Overview of coil designs for wireless charging of electric vehicle," in *Proc. IEEE PELS Workshop Emerg. Technol., Wireless Power Transf. (WoW)*, May 2017, pp. 1–6.
[7] S. Chowdhury, E. Gurpinar, G.-J. Su, T. Raminosoa, T. A. Burress, and B. Ozpineci, "Enabling technologies for compact integrated electric drives for automotive traction applications," in *Proc. IEEE Transp. Electrific. Conf. Expo (ITEC)*, Jun. 2019, pp. 1–8.
[8] Y. Liu, A. Kamineni, H. Ukegawa, E. M. Dede, and J. S. Lee, "Multi-layer design and power transfer test of PCB-based coil for electric vehicle wireless charging," in *Proc. IEEE Wireless Power Technol. Conf. Expo (WPTCE)*, Jun. 2023, pp. 1–5.
[9] P. Dowell, "Effects of eddy currents in transformer windings," *Proc. Inst. Elect. Engineers*, vol. 113, no. 8, pp. 1387–1394, Aug. 1966. [Online]. Available: https://digital-library.theiet.org/content/journals/10.1049/piee.1966.0236
[10] A. Rand, "Inductor size vs. Q: A dimensional analysis," *IEEE Trans. Compon. Parts*, vol. CP-10, no. 1, pp. 31–35, Mar. 1963. [Online]. Available: https://api.semanticscholar.org/CorpusID:110565109
[11] J. Li, T. Abdallah, and C. R. Sullivan, "Improved calculation of core loss with non-sinusoidal waveforms," in *Proc. IEEE Industry Appl. Conf. Conf. Record, 36th IAS Annu. Meeting*, vol. 4, Chicago, IL, USA, 2001, pp. 2203–2210, doi: 10.1109/IAS.2001.955931.
[12] T. Nakamura, "Snoek's limit in high-frequency permeability of polycrystalline Ni–Zn, Mg–Zn, and Ni–Zn–Cu spinel ferrites," *J. Appl. Phys.*, vol. 88, no. 1, pp. 348–353, Jul. 2000.
[13] W.-J. Gu and R. Liu, "A study of volume and weight vs. frequency for high-frequency transformers," in *Proc. IEEE Power Electron. Specialist Conf.*, Jun. 1993, pp. 1123–1129. [Online]. Available: https://api.semanticscholar.org/CorpusID:109478216

[14] D. J. Perreault, J. Hu, J. M. Rivas, Y. Han, O. Leitermann, R. C. N. Pilawa-Podgurski, A. Sagneri, and C. R. Sullivan, "Opportunities and challenges in very high frequency power conversion," in *Proc. 24th Annu. IEEE Appl. Power Electron. Conf. Expo.*, Feb. 2009, pp. 1–14.
[15] M. D'Antonio, S. Chakraborty, and A. Khaligh, "Planar transformer with asymmetric integrated leakage inductance using horizontal air gap," *IEEE Trans. Power Electron.*, vol. 36, no. 12, pp. 14014–14028, Dec. 2021.
[16] J. Biela and J. W. Kolar, "Electromagnetic integration of high power resonant circuits comprising high leakage inductance transformers," in *Proc. IEEE 35th Annu. Power Electron. Specialists Conf.*, Jun. 2004, pp. 4537–4545.
[17] M. Mu, L. Xue, D. Boroyevich, B. Hughes, and P. Mattavelli, "Design of integrated transformer and inductor for high frequency dual active bridge GaN charger for PHEV," in *Proc. IEEE Appl. Power Electron. Conf. Expo. (APEC)*, Mar. 2015, pp. 579–585.
[18] Y. Liu, H. Wu, J. Zou, Y. Tai, and Z. Ge, "CLL resonant converter with secondary side resonant inductor and integrated magnetics," *IEEE Trans. Power Electron.*, vol. 36, no. 10, pp. 11316–11325, Oct. 2021.
[19] J. H. Spreen, "Electrical terminal representation of conductor loss in transformers," *IEEE Trans. Power Electron.*, vol. 5, no. 4, pp. 424–429, Oct. 1990.
[20] R. B. Beddingfield, S. Samanta, M. S. Nations, I. Wong, P. R. Ohodnicki, and S. Bhattacharya, "Analysis and design considerations of a contactless magnetic plug for charging electric vehicles directly from the medium-voltage DC grid with arc flash mitigation," *IEEE J. Emerg. Sel. Topics Ind. Electron.*, vol. 1, no. 1, pp. 3–13, Jul. 2020.
[21] I. Okasili, A. Elkhateb, and T. Littler, "A review of wireless power transfer systems for electric vehicle battery charging with a focus on inductive coupling," *Electronics*, vol. 11, no. 9, p. 1355, Apr. 2022.
[22] J. Shin, S. Shin, Y. Kim, S. Ahn, S. Lee, G. Jung, S.-J. Jeon, and D.-H. Cho, "Design and implementation of shaped magnetic-resonance-based wireless power transfer system for roadway-powered moving electric vehicles," *IEEE Trans. Ind. Electron.*, vol. 61, no. 3, pp. 1179–1192, Mar. 2014.
[23] A. M. Jawad, H. M. Jawad, R. Nordin, S. K. Gharghan, N. F. Abdullah, and M. J. Abu-Alshaeer, "Wireless power transfer with magnetic resonator coupling and sleep/active strategy for a drone charging station in smart agriculture," *IEEE Access*, vol. 7, pp. 139839–139851, 2019.
[24] K. Shi, C. Tang, Z. Wang, X. Li, Y. Zhou, and Y. Fei, "A magnetic integrated method suppressing power fluctuation for EV dynamic wireless charging system," *IEEE Trans. Power Electron.*, vol. 37, no. 6, pp. 7493–7503, Jun. 2022.
[25] J. Van Mulders, D. Delabie, C. Lecluyse, C. Buyle, G. Callebaut, L. Van der Perre, and L. De Strycker, "Wireless power transfer: Systems, circuits, standards, and use cases," *Sensors*, vol. 22, no. 15, p. 5573, Jul. 2022.
[26] H. L. Li, A. P. Hu, and G. A. Covic, "A direct AC–AC converter for inductive power-transfer systems," *IEEE Trans. Power Electron.*, vol. 27, no. 2, pp. 661–668, Feb. 2012.
[27] J. A. Ansari, C. Liu, and S. A. Khan, "MMC based MTDC grids: A detailed review on issues and challenges for operation, control and protection schemes," *IEEE Access*, vol. 8, pp. 168154–168165, 2020.
[28] W. Kabbara, M. Bensetti, T. Phulpin, A. Caillierez, S. Loudot, and D. Sadarnac, "A control strategy to avoid drop and inrush currents during transient phases in a multi-transmitters DIPT system," *Energies*, vol. 15, no. 8, p. 2911, Apr. 2022.
[29] J.-U.-W. Hsu, A. P. Hu, and A. Swain, "A wireless power pickup based on directional tuning control of magnetic amplifier," *IEEE Trans. Ind. Electron.*, vol. 56, no. 7, pp. 2771–2781, Jul. 2009.
[30] H. H. Wu, A. Gilchrist, K. D. Sealy, and D. Bronson, "A high efficiency 5 kW inductive charger for EVs using dual side control," *IEEE Trans. Ind. Informat.*, vol. 8, no. 3, pp. 585–595, Aug. 2012.
[31] K. Stoyka, N. Femia, and G. Di Capua, "Power inductors behavioral modeling revisited," *IEEE Trans. Circuits Syst. I, Reg. Papers*, vol. 67, no. 12, pp. 5636–5649, Dec. 2020.
[32] J. Cale, S. D. Sudhoff, and L.-Q. Tan, "Accurately modeling EI core inductors using a high-fidelity magnetic equivalent circuit approach," *IEEE Trans. Magn.*, vol. 42, no. 1, pp. 40–46, Jan. 2006.
[33] Z. Song, C. Liu, Y. Chen, and R. Huang, "Air-gap permeance and reluctance network models for analyzing vibrational exciting force of in-wheel PMSM," *IEEE Trans. Veh. Technol.*, vol. 71, no. 7, pp. 7122–7133, Jul. 2022.
[34] M. Frivaldsky, M. Pipiska, M. Zurek-Mortka, and D. Andriukaitis, "PFC inductor design considering suppression of the negative effects of fringing flux," *Appl. Sci.*, vol. 12, no. 13, p. 6815, Jul. 2022.
[35] O. C. Onar, S. L. Campbell, L. E. Seiber, C. P. White, and M. Chinthavali, "Vehicular integration of wireless power transfer systems and hardware interoperability case studies," in *Proc. IEEE Energy Convers. Congr. Expo. (ECCE)*, Sep. 2016, pp. 1–8.

SHAHID AZIZ KHAN (Graduate Student Member, IEEE) received the bachelor's degree from the National University of Sciences and Technology, Pakistan, and the master's degree in power systems and automation from North China Electric Power University, Beijing, China. He is currently pursuing the Ph.D. degree with the Department of Electrical and Computer Engineering, University of Michigan-Dearborn. His research interest includes high-power density power electronics converters for electrified transportation applications.

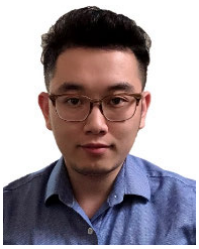

YANGHE LIU (Member, IEEE) received the B.S. and M.S. degrees in mechanical engineering from Purdue University, West Lafayette, IN, USA, in 2013 and 2015, respectively. He is currently a Scientist with the Electronics Research Department, Toyota Research Institute of North America (TRINA), Ann Arbor, MI, USA. He has authored or coauthored over 20 papers in archival journals and conference proceedings. He holds over 15 issued patents. His research interests include mobility development, smart charging, advanced wireless charging systems, advanced electronics packaging, cooling solutions, and machine learning.

MENGQI WANG (Senior Member, IEEE) received the B.S. degree in electrical engineering from Xi'an Jiaotong University, Xi'an, in 2009, and the Ph.D. degree in electrical engineering from North Carolina State University, Raleigh, NC, USA, in 2014. She is currently an Associate Professor with the Department of Electrical and Computer Engineering, University of Michigan-Dearborn. Her research interests include DC/DC and DC/AC power conversions, high efficiency and high power-density power supplies, renewable energy systems, and wide-bandgap power device applications. She is an Associate Editor of IEEE TRANSACTIONS ON POWER ELECTRONICS and IEEE OPEN JOURNAL OF CIRCUITS AND SYSTEMS.

GUANLIANG LIU (Student Member, IEEE) received the B.S. degree from the Department of Electrical Engineering, Beihang University, Beijing, China, in 2016, and the Ph.D. degree from the University of Michigan-Dearborn. His research interests include high-efficiency motor drive and motor design, high-efficiency and high-power density chargers, and wide-bandgap device power device applications.

JAE SEUNG LEE received the master's and Ph.D. degrees from UC Davis, CA, USA, in 2004 and 2005, respectively. He is currently a Senior Manager of the Electronics Research Department and Research Strategy Office, Toyota Research Institute of North America, Ann Arbor, Michigan. He has been leading research and development projects of LIDAR and radar sensor for autonomous driving, power electronics projects for EV charging, energy management, and wireless charging. He now takes responsibility of research strategy and electronics research of the Toyota Research Institute of North America. He received three Research and Development-100 Awards. He is the author or coauthor of over 50 technical articles and issued over 50 patents.

ABHILASH KAMINENI (Member, IEEE) received the B.E. degree (Hons.) in electrical engineering and the Ph.D. degree in power electronics from The University of Auckland, Auckland, New Zealand, in 2012 and 2017, respectively. He joined the Power Electronics Laboratory, Utah State University, Logan, UT, USA, as a Postdoctoral Fellow and an Assistant Professor, in 2017 and 2019, respectively. His main research interests include wireless power transfer and resonant converters.

SHIVAM CHATURVEDI received the B.Tech. degree in electrical and electronics engineering from Gautam Buddha Technical University, Lucknow, India, in 2013, the M.E. degree in area of power electronics from the Shri Govindram Seksaria Institute of Technology Indore, Indore, India, in 2015, and the Ph.D. degree in area of power electronics from the Indian Institute of Technology Jodhpur, Jodhpur, India, in 2021. He is currently a Research Investigator with the Department of Electrical and Computer Engineering, University of Michigan-Dearborn, USA. His research interests include DC microgrids control, virtual impedance shaping, DC/AC power electronic interfaces, and electric vehicle motor control.